Micron 151 (2021) 103152

Contents lists available at ScienceDirect

Micron

journal homepage: www.elsevier.com/locate/micron

Morphological and mechanical changes induced by quercetin in human T24 bladder cancer cells

Bruno Silveira Adami [a,1], Fernando Mendonça Diz [b,d,1], Gustavo Petry Oliveira Gonçalves [c], Camille Kirinus Reghelin [e], Matheus Scherer [e], Artur Pereira Dutra [d], Ricardo Meurer Papaléo [f], Jarbas Rodrigues de Oliveira [e], Fernanda Bueno Morrone [d], Andrea Wieck [a,*], Léder Leal Xavier [a,c]

[a] Laboratório de Biologia Celular e Tecidual, Pontifícia Universidade Católica do Rio Grande do Sul, PUCRS, Avenida Ipiranga, 6681, Porto Alegre, RS, CEP: 90619-900, Brazil
[b] Pós-Graduação em Engenharia e Tecnologia de Materiais, Pontifícia Universidade Católica do Rio Grande do Sul, PUCRS, Avenida Ipiranga, 6681, Porto Alegre, RS, CEP: 90619-900, Brazil
[c] Laboratório Central de Microscopia e Microanálise (LabCeMM), Pontifícia Universidade Católica do Rio Grande do Sul, PUCRS, Avenida Ipiranga, 6681, Porto Alegre, RS, CEP: 90619-900, Brazil
[d] Laboratório de Farmacologia Aplicada, Pontifícia Universidade Católica do Rio Grande do Sul, PUCRS, Avenida Ipiranga, 6681, Porto Alegre, RS, CEP: 90619-900, Brazil
[e] Laboratório de Pesquisa em Biofísica Celular e Inflamação, Pontifícia Universidade Católica do Rio Grande do Sul, PUCRS, Avenida Ipiranga, 6681, Porto Alegre, RS, CEP: 90619-900, Brazil
[f] Centro Interdisciplinar de Nanociências e Micro-Nanotecnologia – NanoPUCRS, Pontifícia Universidade Católica do Rio Grande do Sul, PUCRS, Avenida Ipiranga, 6681, Porto Alegre, RS, CEP: 90619-900, Brazil

ARTICLE INFO

Keywords:
Atomic force microscopy
Quercetin
Bladder cancer
T24 cells
Nuclear morphometry analysis

ABSTRACT

Quercetin is a flavonoid found in a great variety of foods such as vegetables and fruits. This compound has been shown to inhibit the proliferation of various types of cancer cells, as well as the growth of tumors in animal models. In the present study, we analyze morphological and mechanical changes produced by quercetin in T24 bladder cancer cells. Decreased cell viability and cell number were observed following quercetin treatment at 40 μM and 60 μM, respectively, as observed by the MTT assay and trypan blue exclusion test, supporting the hypothesis of quercetin anticancer effect. These assays also allowed us to determine the 40, 60, and 80 μM quercetin concentrations for the following analyses, Lactate Dehydrogenase assay (LDH); Nuclear Morphometric Analysis (NMA); and atomic force microscopy (AFM). The LDH assay showed no cytotoxic effect of quercetin on T24 cancer cells. The AFM showed morphological changes following quercetin treatment, namely decreased cell body, cytoplasmic retraction, and membrane condensation. Following quercetin treatment, the NMA evidenced an increased percentage of nuclei characteristic to the apoptotic and senescence processes. Cells also presented biophysical alterations consistent with cell death by apoptosis, as increased roughness and aggregation of membrane proteins, in a dose-dependent manner. Cellular elasticity, obtained through force curves, showed increased stiffness after quercetin treatment. Data presented herein demonstrate, for the first time, in a quantitative and qualitative form, the morphological and mechanical alterations induced by quercetin on bladder cancer cells.

1. Introduction

Bladder cancer (BC) is the second most common urinary tract malignancy, being the ninth most common cancer in the world, with 430,000 new cases annually (Antoni et al., 2017; Ferlay et al., 2013). When diagnosed early, most cases correspond to non-muscle invasive

* Corresponding author at: Laboratório de Biologia Celular e Tecidual, Escola de Ciências da Saúde e da Vida, PUCRS, Avenida Ipiranga, 6681, Prédio 12, Sala 104, Porto Alegre, RS, CEP:90619-900, Brazil.
E-mail address: andrea.wieck@edu.pucrs.br (A. Wieck).
[1] These authors contributed equally to this work.

https://doi.org/10.1016/j.micron.2021.103152
Received 4 March 2021; Received in revised form 21 July 2021; Accepted 21 September 2021
Available online 23 September 2021

bladder carcinoma (NMIBC), which is associated with a good prognosis (Rockenbach et al., 2013). However, this type of tumor can evolve and invade the lamina propria, becoming classified as muscle-invasive bladder carcinoma (MIBC) (Buss et al., 2018; Moch et al., 2016). MIBC corresponds to 21–50 % of bladder cancer cases (van de Putte et al., 2018), and is associated with poor prognosis and greater lethality (Bambury and Rosenberg, 2013; Bellmunt and Petrylak, 2012). In this case, radical cystectomy is the gold standard surgical treatment (Jacobs et al., 2010; Russell et al., 2016). However, this treatment is associated with high morbidity rates and post-surgical complications (Antoni et al., 2017; Kamat et al., 2016; Russell et al., 2016; van den Bosch and Alfred Witjes, 2011). An alternative therapeutic approach consists of a combination of surgery (bladder tumor transurethral resection), chemotherapy, and radiation therapy (Dietrich et al., 2018; Kamat et al., 2016; Shukla and Kulkarni, 2002). Nevertheless, chemotherapy and radiotherapy are associated with several side effects (Pi et al., 2016).

Therefore, the search for efficient strategies capable of eliminating cancer cells while preserving healthy cells is one of medicine's greatest challenges. In this context, phytochemistry has been widely explored (Lei et al., 2018; Ma et al., 2017; Raffa et al., 2017). One of the most promising phytochemical products is quercetin, which has been shown to have therapeutic potential in the prevention and treatment of several chronic diseases, including neurodegenerative diseases, and cancer (Lesjak et al., 2018). Quercetin is an abundant and easily extracted bioflavonoid found in a variety of fruits, vegetables, and plants (Zhao et al., 2019). It exhibits antitumor activity associated with apoptosis induction, tumor inhibition, and cell cycle arrest in various tumor cell types, such as breast, ovarian, prostate, pancreas, and glioblastoma (Lan et al., 2019; Lei et al., 2018; Lesjak et al., 2018; Liu et al., 2017; Raffa et al., 2017; Tang et al., 2020; Teekaraman et al., 2019). Moreover, while quercetin is toxic for tumor cells, it has no adverse effects on non-cancer cells (Chowdhury et al., n.d.; Pi et al., 2016)

Despite that, there are few studies in the literature demonstrating the effects of quercetin on bladder cancer cells (Ma, 2006; Rockenbach et al., 2013; Tsai et al., 2019). Studies using the human bladder cancer cell line T24 showed that quercetin was able to inhibit cell proliferation (Ma, 2006; Rockenbach et al., 2013), increase the percentage of cells in G0/G, as well as increase caspase 3/7 activity and DNA fragmentation, indicating cell death through apoptosis induction (Ma, 2006; Tsai et al., 2019). Quercetin can also significantly inhibit ecto-5′-nucleotidase/CD73 enzyme activity, which regulates AMP and adenosine extracellular levels, which are cell proliferation factors (Rockenbach et al., 2013).

Atomic force microscopy (AFM) is a non-destructive tool that can provide information about cell morphology and surface (topography), as well as its biophysical properties, at the nanometric scale (Hayashi and Iwata, 2015; Lekka et al., 2012; Pi et al., 2016). This biophysical information can generate important data on tumor cell basic functions and metabolism, closely associated with other cell processes such as adhesion, transformation, and invasiveness (Bastatas et al., 2012; Doss et al., 2015; Hayashi and Iwata, 2015; Kim et al., 2017a). Considering these characteristics, AFM has been explored to assess cell membrane structural integrity and behavior regarding the effects of antitumor drugs (Li et al., 2008; Qu et al., 2018; Sundar Rajan et al., 2017). The goals of our study were to evaluate, cell viability, proliferation, plasmatic membrane integrity, nuclear morphometry, and biophysical changes in T24 cells treated with different concentrations of quercetin.

2. Material and methods

2.1. Materials

The reagents used in cell culture were RPMI-1640, fetal bovine serum (FBS), penicillin-streptomycin (10,000 U/mL), amphotericin B (Fungizone®), and 0.5 % trypsin/EDTA solution, obtained from Gibco Laboratories (Carlsbad, USA). For biological assays, quercetin (≥95 %, HPLC), paraformaldehyde, and Hoechst 33,258 were purchased from Sigma-Aldrich (St. Louis, USA). Trypan blue was from Gibco Laboratories (Carlsbad, USA) and the MTT (3-(4,5-dimethylthiazol-2-yl)-2,5-diphenyltetrazolium bromide solution – MTT 5 mg/mL in PBS and 90 % culture medium supplemented with 10 % FBS) from Sigma-Aldrich (Ontario, Canada), and calcium and magnesium-free medium (CMF, from our laboratory). The Lactate dehydrogenase (LDH) kit was purchased from Labtest (Minas Gerais, Brazil).

2.2. Experimental design

The experiments were performed sequentially with different objectives (selection of quercetin concentration, evaluation of cell membrane integrity, investigation of dynamic tumor cell fitness after exposure to quercetin, and evaluation of structural characteristics by AFM). Each specific experimental test was a prerequisite to subsequent assay, as schematically represented in the experimental design conducted (Fig. 1).

For each experimental procedure, cells were trypsinized, counted on a hemocytometer, and plated at the appropriate density according to the experimental protocol.

2.3. Cell culture and Preparation of quercetin for treatment

Human bladder cancer cell line T24 was obtained from the ATCC (American Type Culture Collection). Cells were grown in RPMI-1640 medium supplemented with 10 % FBS, 0.5 U/mL penicillin/streptomycin (Gibco), and 0.1 % (v/v) fungizone. T24 cells were maintained in an incubator at 37 °C, with 95 % relative humidity and 5% CO_2 atmosphere. Quercetin was kept at room temperature and first diluted in RPMI-1640 at a 500 μM concentration followed by a serial dilution to desired concentrations (10, 20, 40, 60, and 80 μM). To ensure the suspension uniformity, they were stirred on vortex agitation before every use.

2.4. Cell viability (MTT assay)

Cell viability was assessed using the MTT assay. Briefly, since the reduction of MTT salt into formazan only occurs in metabolically active cells any increase or decrease in the number of viable cells can be detected using optical density to measure the formazan concentration (Alban et al., 2020). For MTT assay, T24 cells were seeded at a density of 5×10^3 cells per well in 96-well plates and maintained in an incubator for 24 h. After confluence, T24 cells were treated with different concentrations of quercetin and incubated for 24 and 48 h. Control cells were treated with medium only. Following the 24 and 48 h treatment periods, the medium was removed and the cells washed with PBS (pH = 7.4), followed by the addition of 100 μL of 0.5 % MTT solution per well. After 4 h. of incubation, the medium was removed and the plate was kept at room temperature for 24 h, for drying purposes. Afterwards, formazan crystals were eluted in 100 μL DMSO (Sigma-Aldrich, 995%). Optical staining density was determined using a spectrophotometer (SpectraMax Plus) at 570 nm. Three independent experiments were performed for each concentration, all in triplicate. Results were determined as a percentage of absorbance from quercetin treated cells compared to control cells (non-treated).

2.5. Cell proliferation assay

To determine the number of viable cells following quercetin treatment, cells were counted and judged viable based on their ability to exclude Trypan Blue. For this evaluation, T24 cells were plated at a density of 10×10^3 cells per well in 24-well plates and treated with fresh medium containing different quercetin concentrations (40, 60, and 80 μM) along 24 and 48 h. Concentrations used in this assay were based on MTT assay results showing the antitumor effects of quercetin against

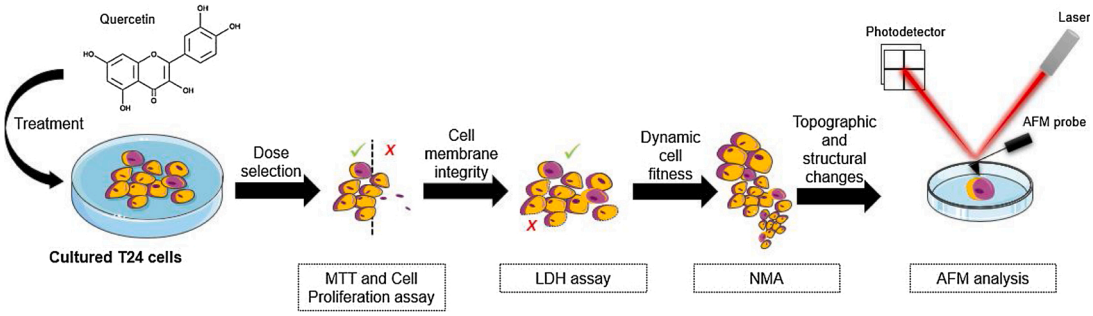

Fig. 1. Representation of the experimental design conducted during the study.

T24 cancer cells. After the quercetin treatment period, culture medium was removed, and cells were washed with CMF followed by the addition of 0.5 % trypsin/EDTA to ensure cell dissociation. After trypsin neutralization in culture medium, cells were marked with trypan blue and immediately counted in a Cell Counter - Life Technologies. Three independent experiments were performed for each concentration, all of these in triplicate. Results are expressed as a percentage of living cells compared to the control group.

2.6. Lactate dehydrogenase assay (LDH assay)

The LDH assay was performed to assess the cell membrane integrity of T24 cells since LDH release in the culture medium is evidence of membrane rupture. T24 cells were seeded at a density of 10×10^3 cells per well in 24-well plates and incubated with quercetin (40, 60, and 80 μM) for 24 h. Enzyme activity was measured in the supernatant and cell lysate using the colorimetric assay Lactate Dehydrogenase kit (Labtest, Minas Gerais, Brasil). For cell lysis control, 5% Tween was used. LDH release was calculated by measuring the absorbance at 492 nm using an ELISA microplate reader. Three independent experiments were performed for each concentration, all of these in triplicate.

2.7. Nuclear morphometry analysis (NMA)

The analysis of the nuclear size and irregularity was performed to investigate the dynamic cell fitness involved in cell populations after exposure to quercetin (i.e., apoptosis, senescence, or mitotic catastrophe) based on nuclear shape and size. The NMA assay was performed according to Filippi-Chiela and colleagues (2012). T24 cells were seeded at a density of 10×10^3 cells per well in a 24-well plate and treated with quercetin (40, 60, and 80 μM) for 24 h. After the treatment period, cells were washed with PBS, and fixed with 4% formaldehyde for 20 min, washed once again with PBS, and stained with Hoechst 33,342 at a 1:1000 dilution in PBS, for 10 min, in the dark. Images were acquired in a fluorescence microscope (at 100x magnification), followed by analysis in the Image-Pro Plus 6.0 software (IPP6, Media Cybernetics - USA). The nuclear contours were delimited using the magic wand tool, proceeding with the acquisition of the following variables: area, Radiusratio (Rr), Roundness (Rou), Aspect (Asp), and Areabox (Arbx). Raw data were then analyzed using the NMA spreadsheet (available at: http://www.ufrgs.br/labsinal/NMA/), in which the Nuclear Irregularity Index (NII) is calculated for each nucleus, through the following equation:

$$NII = 0.9\ x\ Asp - 0.87\ x\ Arbx + 0.96\ x\ Rr + 0.92\ x\ Rou$$

Different nuclear phenotypes were separated in an area versus nuclear irregularity index (NII) plot and control-cell nuclei were used to set the normal parameters. Based on this plot, nuclei were classified as normal (N), small and regular (SR), small and irregular (SI), large and regular (LR), and large and irregular (LI) (ADD Filippi-Chiela et al. (2012) and Vargas et al. (2020). SR nuclei typically correspond to apoptotic cells, and SI nuclei to damaged mitotic cells, while LR and LI correspond to nuclei from senescent cells.

2.8. Atomic force microscopy (AFM)

An atomic force microscope (Dimension Icon, Bruker) was used to investigate the topographic and structural changes in T24 cells treated with different concentrations of quercetin (40, 60, and 80 μM). The AFM probe (f_0: 70 kHz; k: 0.4 N/m, half-angle (α): 18°; ScanAsyst-Air, Bruker) was calibrated using the thermal tune method. Furthermore, a deflection sensitivity value of 51 nm/V was found based on the average from 10 measurements (for each probe) obtained by force spectroscopy on a standard sapphire sample, resulting in the elastic constant of the mean value of 0.34 N/m. Furthermore, only one AFM probe was used for the topographic analyses (one AFM probe for each sample group), and one probe/each cell for the force spectroscopy analyses.

2.8.1. AFM sample preparation

For AFM analysis, T24 cells were plated at a density of 10×10^3 cells per glass coverslip (18 mm diameter) accommodated in a 12-well plate for 24 h. After this period, cells were treated with quercetin (40, 60, and 80 μM) for another 24 h. Following quercetin treatment, cells were washed with PBS (3x) and fixed in 4% paraformaldehyde (for 10 min), and then washed with PBS again (3x) (Kim et al., 2017b). The samples were carefully air-dried and taken for immediate analysis.

2.8.2. AFM imaging of T24 cells: Topography, roughness, and particle size

The acquisition of topographic images was performed with at least 10 different cells (60 × 60 μm, 512 × 512 pixels, and scanning frequency of 0.5 Hz) for each sample group (control and treatment). For analysis of cell ultrastructure, 3 images (1 × 1 μm, 256 × 256 pixels, and scanning frequency of 1 Hz) were collected for each analyzed cell. Both analyses were performed in peak force tapping mode, in which the probe was set to oscillate at 2 kHz with a peak-to-peak amplitude of 300 nm. The recursive algorithm ScanAsyst (Bruker) was also used to adjust the values of the Integral Gain and Setpoint (for better control of the interaction strength between probe and sample) (Trtik et al., 2012).

Roughness (Ra and Rq) and particle size data were obtained from ultrastructure images in the NanoScope Analysis 1.5 software (Bruker). Data collection for Ra, Rq, and particle size analyses were obtained before and after treatment with the *Flatten* command (first-order). The ultrastructure measurements of T24 cells were all obtained from the areas surrounding the nuclei, and the height of the cells was obtained through the *step* analysis function (mapping the mean of 51 lines of cell profile) under the same conditions.

2.8.3. Force curves and elastic modulus analysis

The analysis of force measurements was performed on 10 cells from each sample group (cells with a non-characteristic appearance or the presence of crystal formation were avoided). Thus, a measurement per single cell, in a central area of the nucleus, was performed (Codan et al., 2014). The force curves were obtained from the deflection changes (δ) when the probe applied a given force (F) on the sample, which is related

to the spring constant (k). The Sneddon model was used for a conical indenter to obtain the elastic modulus values (Sneddon, 1965), as shown in the following equation:

$$F = 2/\pi \bullet E/(1 - v^2) \bullet \delta^2 \tan(\alpha)$$

Where F is the applied force, δ is the change in the deflector, E is the elastic modulus of the sample, v is the Poisson's ratio, and α is the half-angle of the probe. To calculate the elasticity of the cells, a Poisson's ratio value of 0.5 is generally used (Pi et al., 2016). The choice of this model is justified by the heterogeneity of the cell structure, in addition to considering the deformation caused by the probe. The *engage* parameter (approximation of the probe to the surface of the sample) took place with an approximate speed of 0.5um/s (to avoid possible distortions in the curves obtained). The Ramp function of the NanoScope 8.15 was used to obtain the force curves (scan size of 1000 nm, Trig threshold of 0.1 V, ramp rate of 1 Hz, and n = 512). The indentation velocity was maintained close to 1 μm/s for all samples, and the *loading rate* varied between the groups (2.7, 12.8, 51.5, and 43.8 n/s for control, 40, 60, and 80 μM, respectively). In the NanoScope Analysis software, the curves obtained were submitted to baseline correction (baseline correction) and adjustment of the contact point (contact point) to obtain the elastic module value (Supplementary Fig. 1). The indentation observed through the curves was 299.4 ± 116 nm (control), 282.0 ± 62.2 nm (40 μM), 315.7 ± 46 nm (60 μM), and 247.9 ± 74.2 nm (80 μM). For more detailed information refer to supplementary table 1.

2.9. Statistical analysis

Results are expressed as mean ± standard error. Cell viability and proliferation were analyzed by Two-Way ANOVA, while LDH, Ra, Rq, and Young Modulus were analyzed by One-Way ANOVA followed by Tukey's post hoc. *P*-values less than 0.05 were considered significant. For the NMA results, Student's *t*-test was performed. All statistical analyses were performed in Prism 8 software.

3. Results

3.1. Quercetin effect on T24 cells proliferation

Five quercetin concentrations (10, 20, 40, 60 and 80 μM), and two different exposure times (24 and 48 h) were tested to determine the parameters to be used in the following experimental procedures of our study. Changes in tumor viability and cell number were assessed using MTT assay and cell counting by Trypan blue exclusion method. Quercetin effects on T24 cell line viability and proliferation are shown in Fig. 2. A significant effect of quercetin concentration was observed as reduced cell viability in both treatment periods ($F_{7,176} = 71.089$; $p < 0.0001$ – Fig. 2A). Cells treated with quercetin for 24 h showed a reduced viability starting at 60 μM concentration ($t_{7,176} = 5.062$, $p = 0.01$; $t_{7,176} = 7.645$, $p < 0.0001$, for 60 μM and 80 μM, respectively – Fig. 2A). At 48 h of treatment, reduced cell viability became apparent at 80 μM concentration ($t_{7,176} = 14.98$, $p < 0.0001$– Fig. 2A). A significant time-dependent concentration interaction was observed ($F_{7,176} = 7.059$; $p < 0.0001$) starting at 80 μM, where the effect on T24 cell viability was higher at 48 h of treatment ($t_{7,176} = 5.189$, $p < 0.0001$; $t_{7,176} = 4.949$, $p < 0.0001$ and $t_{7,176} = 3.435$, $p = 0.0059$ for 80 μM, 100 μM and 120 μM respectively– Fig. 2A). In the cell count assay, a significant effect of quercetin was observed ($F_{5,132} = 515.2$; $p < 0.0001$ – Fig. 2B). Cells treated with quercetin for 24 h showed a reduction in the number of viable cells starting at 60 μM ($t_{5,132} = 6.523$, $p = 0.0001$; $t_{5,132} = 21.61$, $p < 0.0001$, for 60 μM and 80 μM, respectively – Fig. 2B). While for the 48 h exposure period, all quercetin concentrations had a significant effect on cell proliferation ($t_{5,132} = 5.744$, $p = 0.0012$; $t_{5,132} = 23.22$, $p < 0.0001$, $t_{5,132} = 32.03$, $p < 0.0001$; for 40 μM, 60 μM and 80 μM, respectively – Fig. 2B).

3.2. Plasmatic membrane integrity

By comparing responses obtained in viability and proliferation assays (Fig. 3), we defined the concentrations and the treatment time to be used in the LDH assay. Therefore, this set of experiments were performed to evaluate plasma membrane integrity after 24 h of treatment with 0, 40, 60, 80 μM quercetin concentrations (Fig. 3). No differences in LDH release were observed among quercetin treatments ($F_{3.12} = 173$; $p = 0.21$), indicating that the plasma membrane was intact.

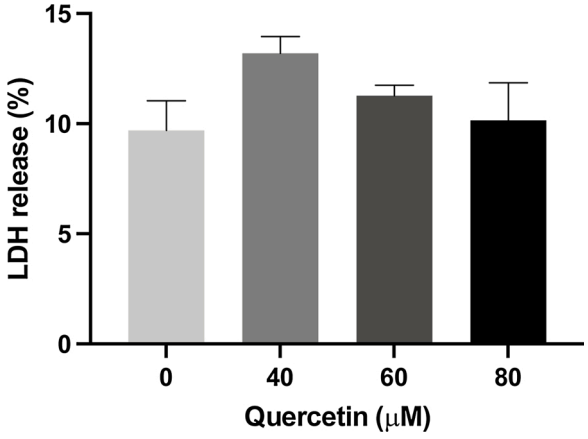

Fig. 3. Quercetin cytotoxic effect assessed by LDH levels released in the supernatant after 24 h of treatment. Results are presented as mean ± SEM of the percentage of LDH released in the supernatant. Control refers to the total percentage of LDH release in culture obtained by cell lysis, without quercetin. Data were analyzed for statistical significance using one-way ANOVA, followed by Tukey's post hoc.

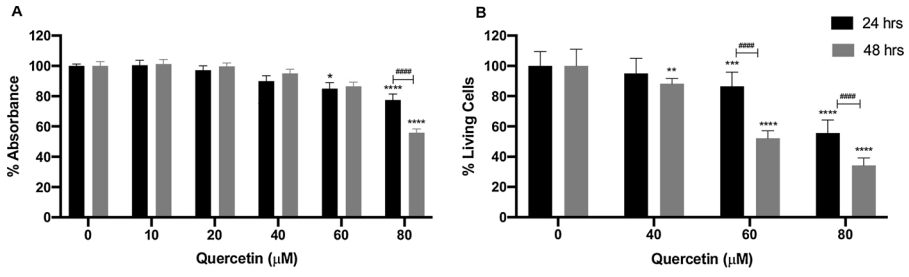

Fig. 2. Quercetin effect on T24 cells viability A) and proliferation B) evaluated by MTT assay and by the Trypan blue exclusion method, respectively. A) the effect of quercetin on cell viability starts at 60 μM/24 h. At 80 μM is possible to observe the difference between 24 and 48 h, where 48 h show a more aggressive cytotoxic effect. The results of this experiment were used to evaluate the concentrations to be used in the following experiments. B) the antiproliferative effect of quercetin starts at 40 μM/48 h. For 60 μM and 80 μM, 48 h. of exposure shows a higher antiproliferative effect. Since no effect of 10 μM and 20 μM concentrations were observed on cell viability, they were not used for MTT analysis. Data presented as mean ± SEM and were analyzed for statistical significance using two-way ANOVA, followed by Tukey's post hoc. * indicates significant difference in comparisons between concentrations x control for each exposure period (****$p < 0.0001$; ***$p < 0.001$; **$p < 0.01$; *$p < 0.05$). # indicates differences in comparisons between different exposure periods for each quercetin concentration ($^{\#\#\#\#}$ $p < 0.001$; $^{\#\#}$ $p < 0.005$).

3.3. Nuclear morphometric analysis

The NMA analysis indicates that treatment with different quercetin concentrations (40, 60 and 80 μM) for 24 h significantly changes the nuclear morphology of T24 cells ($F_{9,8926} = 2932$; $p < 0.0001$ – Fig. 4), observed as a reduced percentage of Normal (N) nuclei as the quercetin concentration is increased ($F_{3.6382} = 19,245$; $p < 0.0001$ – Fig. 4E). The increase in the percentage of LR nuclei also followed quercetin

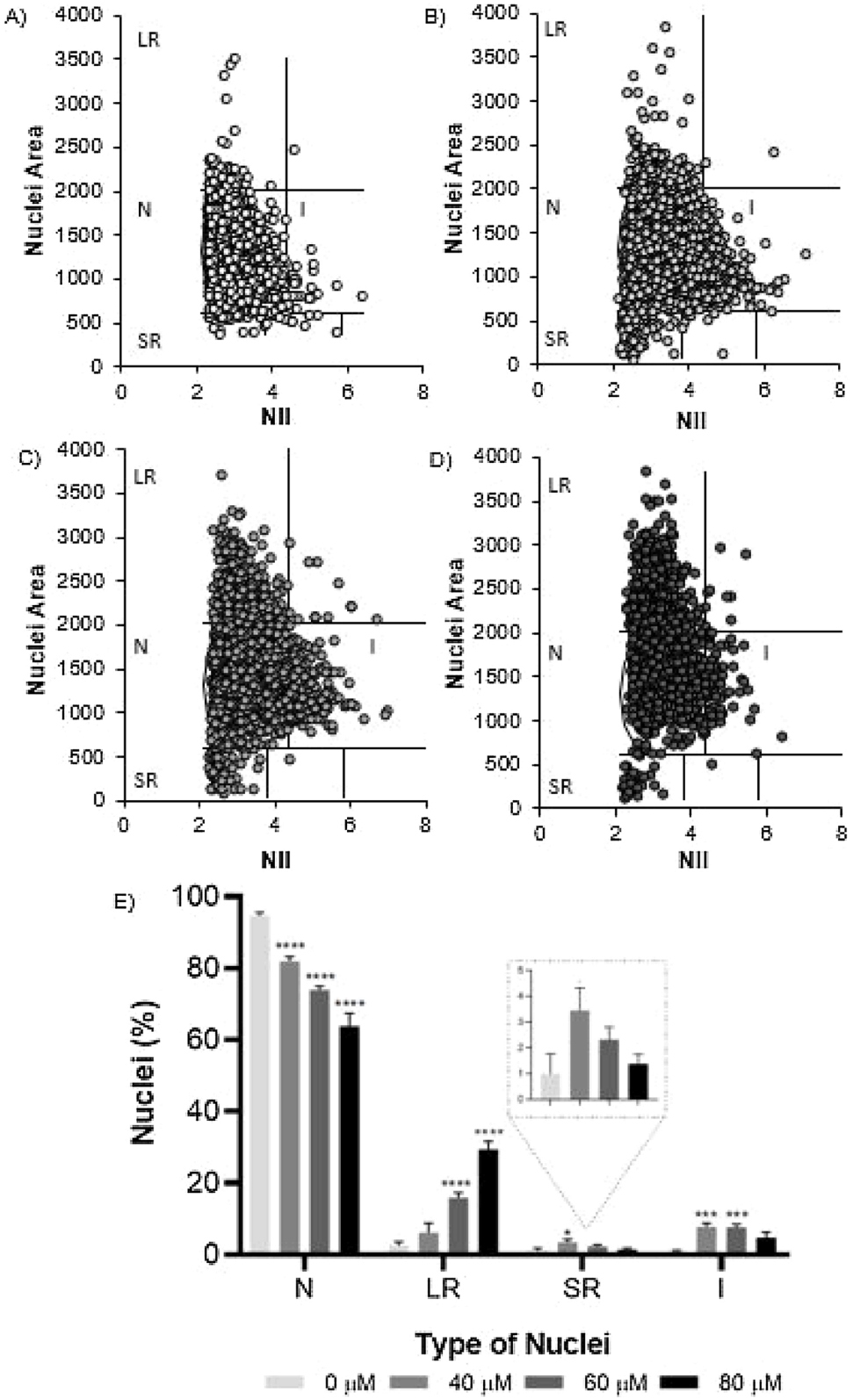

Fig. 4. NMA analysis of T24 cell line treated with different quercetin concentrations for 24 h.: A) 0 μM, B) 40 μM, C) 60 μM and D) 80 μM. E) shows nuclear types distribution in percentages. NII represents the irregularity index: N = regular, LR = large regular, SR = small regular and I irregular. **** $p < 0.0001$;***$p < 0.001$; **$p < 0.01$; * $p < 0.05$.

concentration increase ($F_{3.1221}$ = 1962; $p < 0.0001$ – Fig. 4E). By contrast, the percentage of SR nuclei was reduced with higher concentrations of quercetin, but not differing from control cells. The only concentration that statistically increased the percentage of SR nuclei was 40 μM ($F_{3.267} = 26.70$; $p < 0.0001$ – Fig. 4E). Regarding I nuclei, all concentrations of quercetin lead to an increase in the percentage of this nuclear type compared to control cells ($F_{3.1056} = 516.3$; $p < 0.0001$ – Fig. 4E), with the highest percentages been observed at 40 μM and 60 μM.

3.4. Morphological changes induced by quercetin

Qualitative analysis of cells treated with quercetin showed different morphological alterations according to the concentration used. After exposure to 40 μM quercetin, although cells still retain native characteristics, irregularities and cytoplasmic contour projections, as well as hole-like structures, and a nucleus with the presence of nucleoli, were observed (Fig. 5E, white arrows).

At 60 μM, it is possible to observe cell body shrinkage, with initial cytoplasmic condensation, and plasma membrane retraction as well as an increase in the number of holes and pits. Despite these alterations, the nucleus remains integral, presenting nucleolar structures (Fig. 5G-H). Finally, the 80 μM concentration (Fig. 5J-K), showed collapsed cells with condensed plasma membrane and, in the nucleus, the number of nucleoli is reduced. It is also possible to visualize extruded vesicles with morphological and biophysical characteristics compatible with apoptotic bodies, suggesting ongoing apoptosis (Fig. 5K, hollow arrows). For three-dimensional images refer to Supplementary Fig. 2 in Supplementary Material.

Quantitative analysis of cell heights treated with quercetin showed no significant difference (Fig. 6).

3.5. Ultrastructural changes in the tumor surface caused by quercetin

Alterations in cell membrane after quercetin treatment were accessed via roughness and particle size in cell membrane analysis. For both analyses, 1 μm^2 (1 μm x 1 μm) morphological characterization areas were defined around the nucleus (Fig. 7). The roughness qualitative analysis revealed structures such as holes (Fig. 7 B, D, F and, H - white arrows) and pits (Fig. 7 D, F and, H - black arrows), in a dose-dependent manner, which seems to be closely related to increased roughness of the surface ultrastructure of cells treated with quercetin. Particle size analysis (Fig. 7 I) showed a displacement to the right of points in the graph, also in a dose-dependent manner, indicating an

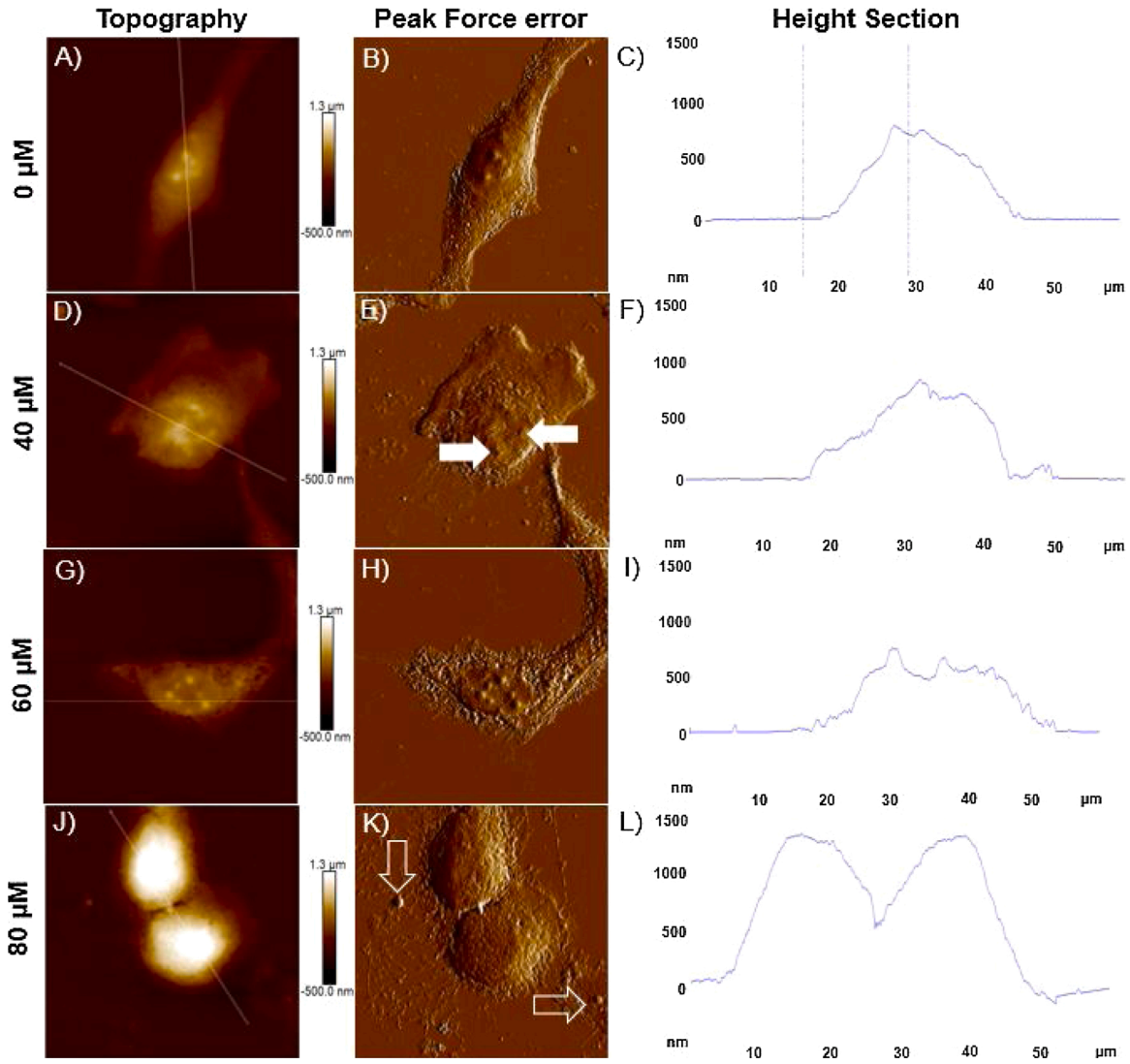

Fig. 5. AFM images of T24 cells treated with different quercetin concentrations for 24 h.: A) and B) 0 μM; D) and E) 40 μM; G) and H) 60 μM; J) and K) 80 μM. Images A), D), G) and J) show the topography of cells, and B), E), H) and K) depict peak force error. C), F), I) and L) shows the height profile of T24 cells. White arrows indicate nucleoli; hollow arrows depict structures similar to apoptotic bodies.

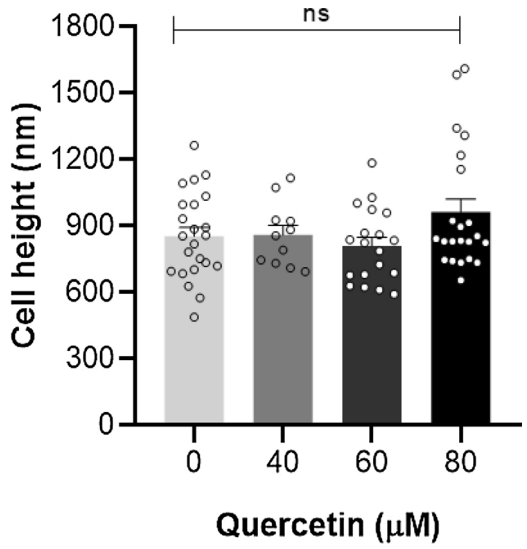

Fig. 6. Quantitative analysis of the mean cross-section of the heights of T24 cells treated with quercetin after 24 h.

increase in particle size and suggesting increased protein aggregation in the membrane, open/closing in ion channels as well as cytoskeleton disruption induced by quercetin.

Subsequently, we performed cell roughness quantitative analysis, using particle size values and mean roughness calculations (Ra), and quadratic roughness (Rq) (Fig. 7 J and K). The Ra analysis demonstrated a statistically significant increase in roughness in a dose-dependent manner ($F_{3,189} = 5434$; $p < 0.0001$), which was also observed for Rq values ($F_{3,189} = 4975$; $p < 0.0001$).

3.6. Quercetin effect on T24 elasticity

The stiffness of T24 human bladder cancer cells was determined by AFM force indentation analysis. The process of approaching and retracting the probe against the surface of the T24 cells is shown in the force-distance curves (Fig. 8), which could be calculated into Young's modulus using the basic Sneddon model.

The effect of quercetin on cell elasticity was inferred by calculating the Young's Modulus. The elasticity of T24 cells was reduced following quercetin treatment at all concentrations. Also, a significant increase in cellular stiffness with increasing concentrations of quercetin was observed (40, 60, and 80 μM) ($F_{3,55} = 4.16$; $p = 0.009$ – Fig. 9).

4. Discussion

Quercetin antitumor activity in human bladder cancer cells has been previously described in the literature due to its antiproliferative effects, inhibiting colony formation, inducing cell death by apoptosis as well as cell cycle arrest in the T24 cell line (Ma, 2006; Rockenbach et al., 2013). Initially, we assessed the effects of quercetin cytotoxic activity on the viability and proliferation of the T24 cell line to determine the proper concentrations and exposure period to be used in further analysis. Thus, five quercetin concentrations (10, 20, 40, 60, and 80 μM) and two different exposure times (24 and 48 h) were tested. Changes in tumor viability and proliferation were assessed using the MTT assay and cell counting by Trypan blue exclusion method. As expected, the higher the concentration and the longer the exposure to quercetin, the greater the action perceived on tumor cells. In an attempt to follow the nuanced morphological transition in membrane ultrastructure caused by quercetin exposure, as well as to preserve the tumor biophysical information associated with cellular physical properties, the 40, 60, and 80 μM concentrations, and 24 h treatment, were chosen.

Our results on cell viability agree with data from the literature, as we observed reduced cell viability following quercetin treatment starting at 60 μM for 24 h of exposure and 80 μM for 48 h. Results obtained in the MTT assay allowed us to outline the concentrations to be evaluated in subsequent assays. In order to determine the antiproliferative activity of quercetin, concentrations of 10 and 20 μM were excluded from the following assays, since they showed no effect on T24 cell viability.

At 24 h of treatment, quercetin concentrations of 60 μM and 80 μM significantly reduced the cell count, while at 48 h, all concentrations tested (40–80 μM) showed the same reduction, an affect also seen with the treatment period (Fig. 2B). The absence of plasma membrane damage suggests that the antiproliferative effect observed here is not related to cellular necrosis, indicating that other mechanisms are involved in quercetin antiproliferative effects (Basso et al., 2019). Subsequent analyses performed by us shed greater light on the mechanisms involved in this process.

Nuclear morphometry (NM) is the quantitative description of the geometric findings of nuclear structure in any dimension (Stevens et al., 2008; Vakifahmetoglu et al., 2008). Several cellular mechanisms are known to affect NM (Stevens et al., 2008; Vakifahmetoglu et al., 2008). Since the reduction in cell number following quercetin treatment was not due to damage to the plasma membrane structure, we used the Nuclear Morphometric Analysis (NMA) to quantify the cell number and its nuclear characteristics, after quercetin treatment. The NMA technique permits the quantification of the number of cells in a population presenting characteristics typically seen in senescence (increased nuclear area), apoptosis (condensation and nuclear fragmentation), as well as other nuclear irregularities related to cell death (Filippi-Chiela et al., 2012) (Fig. 4). Moreover, alterations in microtubule dynamics, chromatin remodeling due to exogenous stress, and alterations in the cell cycle checkpoint can also be detected (Filippi-Chiela et al., 2012; Stevens et al., 2008; Vakifahmetoglu et al., 2008). We evaluated the presence and percentages of N, LR, SR, and I nuclei. Our results demonstrated that as higher the quercetin concentration, the higher the percentage of LR nuclei, an indication of senescence (Filippi-Chiela et al., 2012). Senescence induction, or reactivation, is an important mechanism in anticancer therapy, representing a good target for anticancer drugs. The senescence process is marked by an increase in the nuclear area, which is observed in LR nuclei. This suggests that a possible mechanism by which quercetin reduces cell viability and proliferation is by inducing, or reactivating, senescence processes. The SR nuclei are very condensed and regular, indicating early or intermediate apoptosis (Filippi-Chiela et al., 2012). Our data indicate that cells exposed to 40 μM quercetin might be in early-stage apoptosis since the percentage of SR nuclei in those cells was increased. However, increasing quercetin concentration did not lead to an increase in SR nuclei, and therefore, apoptosis. Lastly, the increase in I nuclei, which are of normal size but highly irregular in shape, indicates other nuclear damaging events (i.e. mitotic catastrophe) may be involved in the reduced cell viability and proliferation induced by quercetin.

Atomic Force Microscopy (AFM), has been shown to be an excellent tool for morphological/topographic elucidation in studies with tumor cells (Hayashi and Iwata, 2015; Kim et al., 2017a; Pi et al., 2015). Due to its nanometric precision, atomic force microscopy can be used to identify subtle changes in morphology, membrane ultrastructure, and biophysical properties. In this way, we observed for the first time, as far as we are aware, the morphological/topographic impact of quercetin antitumor effects in human bladder cancer assessed via AFM. We performed mapping in peak force tapping mode to demonstrate topographic features, and cellular changes at the membrane level of T24 cells exposed to 40, 60, and 80 μM concentrations of quercetin at 24 h of treatment (Fig. 5). Cells unexposed to quercetin were used as a control since they are in their native form (well-outlined cell body, smooth cell membrane, and nucleus presenting nucleolar structures-Fig. 5A and B). Our characterization showed a pattern of damage to the cell body following treatment with different quercetin concentrations, gradually

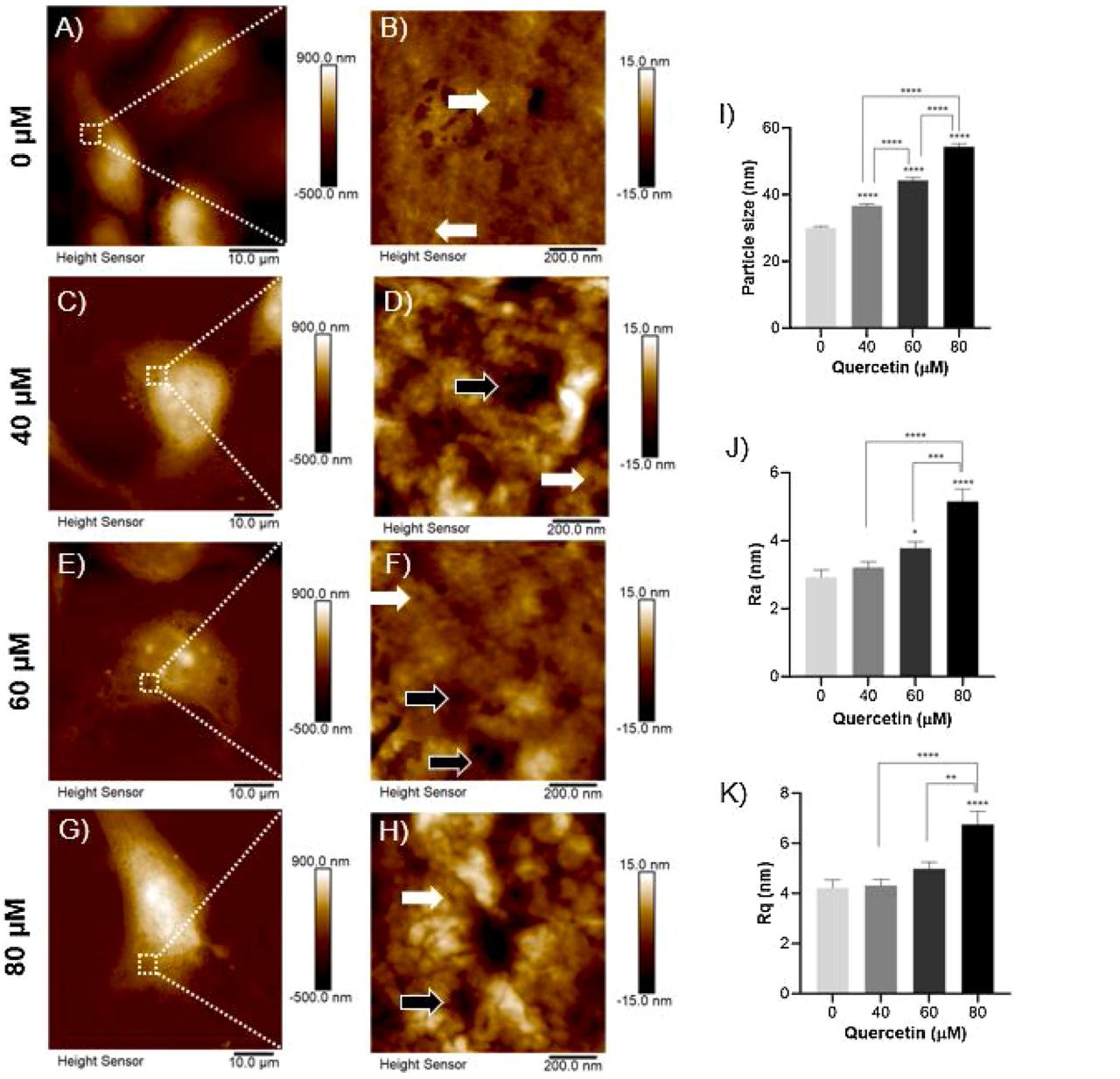

Fig. 7. Ultrastructure analysis through contact scanning by Atomic Force Microscopy (AFM). A) and B) images from control cells; C) and D) cells treated with 40 µM; E) and F) 60 µM, and G) and H) 80 µM quercetin concentration. Images B), D), F) and H) corresponds square-section (1 × 1 µm points) depicted in A),C), E) and G). White arrows indicate holes in the cell membrane, while black arrows indicate pits. Quantitative analysis of T24 cells ultrastructure by AFM: I) Particle size, J) average roughness (Ra), and K) quadratic roughness (Rq), analyzed through the 1 × 1 mm images of T24 cells. Data presented as mean ± SEM and analyzed by one-way ANOVA, followed by Tukey's post hoc ****p < 0,0001, **p < 0.01, *p < 0.05.

starting with small contour irregularities, an increase in the number of holes and pits, cellular shrinkage, culminating in the collapse of the tumor cell (Figs. 5 and 7). Morphological aspects, such as cellular shrinkage observed at 40 and 60 µM quercetin concentrations, have been presented as a hallmark of the apoptotic process (Bortner and Cidlowski, 1998), suggesting that cells treated with quercetin are dying by apoptosis. These findings agree with the literature which describes the apoptotic process morphology (Ziegler and Groscurth, 2004), and with evidence that quercetin can induce apoptosis in different bladder cancer cell lines, including the T24 strain, corroborating our morphological findings (Ma, 2006). The cellular shrinkage related to apoptotic death can also be seen, via AFM, in hepatocellular carcinoma cells treated with American ginseng root extract (Qu et al., 2018). Moreover, the LDH results showing no damage to the cell membrane, and the NMA analyzes, demonstrating the presence of nuclei with apoptotic characteristics, reinforce this hypothesis.

These quantitative data are in accordance with the qualitative analysis, which demonstrated an increase in the number of holes and pits, together with an increase in roughness. Roughness and particle size analyzes are qualitative and quantitative parameters in tumor membrane ultrastructure studies, as it allows cell physiological processes to be related to membrane surface characteristics after treatment with a variety of compounds (Zhang et al., 2014). We used these parameters to assess cell roughness during the anti-tumor process and demonstrate changes in particle size in the cell membrane after quercetin treatment. The Ra and Rq results might reflect the increased formation of holes and pits on the cell surface (Fig. 7), indicating that these structures are responsible for the increased roughness. The formation of holes and pits is probably a result of cytoplasmic retraction and shrinkage of cells, as seen in our morphological analyzes. Along with shrinkage, there is a

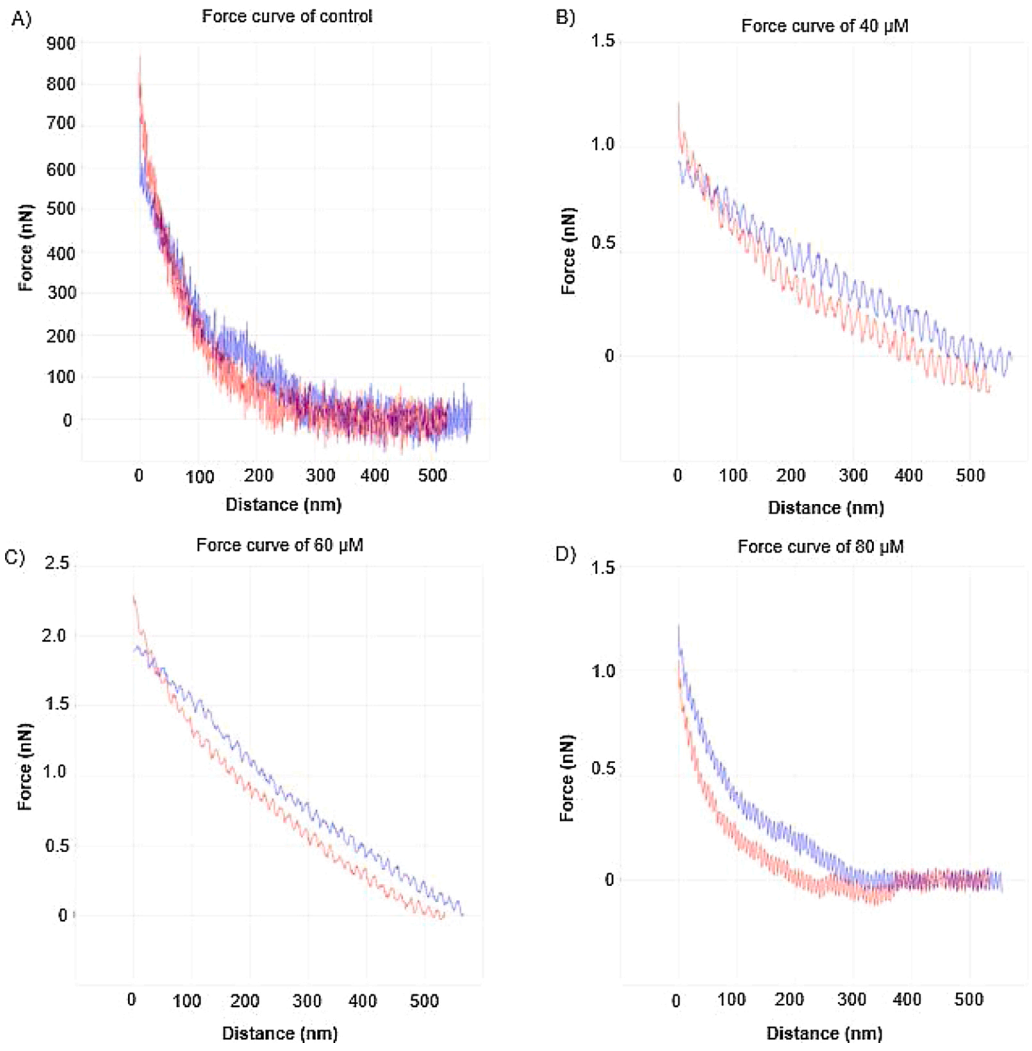

Fig. 8. Effects of quercetin on force-distance curves obtained on T24 cells. A) control cells; B), C) and D) cells treated with 40, 60, and 80 µM of quercetin, respectively. Red line – Approach; Blue line – Retract.

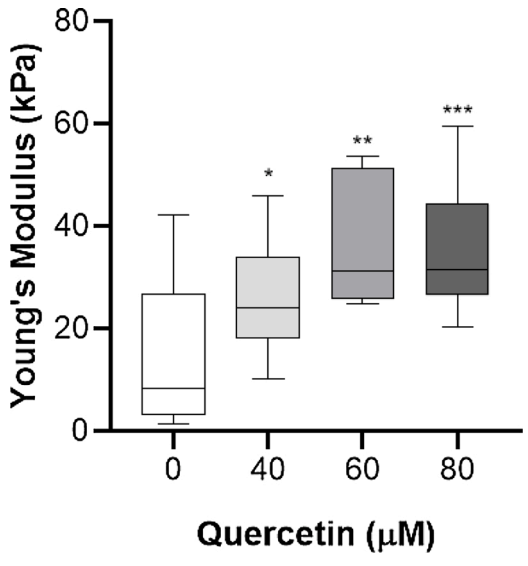

Fig. 9. Quantitative analysis of Young's modulus (kPa) obtained in T24 control cells (Control), and quercetin treated (40, 60, and 80 µM). Data presented as mean ± SEM. ***p < 0,001, p < 0.01, *p < 0.05.

process of loss of osmotic retention capacity observed in apoptotic cells, which would lead the plasma membrane to collapse over cellular structures (Pi et al., 2015). After shrinkage, cytoskeleton organelles and structures show greater compaction which, together with plasma membrane collapse, would lead to the formation of small holes and pits on these compacted structures. It has been previously observed that in withered cells, or those subjected to hypertonic solutions, the apical membrane in the cortex tends to collapse (Pietuch et al., 2013). Moreover, apoptotic cells are generally more rugged as demonstrated in rat monocytes subjected to induced apoptosis. In this study, the author associated the significant increase in cell membrane roughness to the apoptosis process (Wang et al., 2011). In general, after quercetin treatment, an increase in roughness and particle size has been shown to be a hallmark of quercetin's anti-tumor effect on T24 cells. In addition, the rough appearance of the cells can be attributed to the formation of holes and pits, as well as the increase in the size of particulate components of the membrane (Pi et al., 2015).

Cellular elasticity evaluation through AFM has been widely used for the analysis of cancer cell differentiation in both primary and commercial cultures (Cross et al., 2007; Wang et al., 2016). Human cancer cells have been shown to be softer than their respective normal cells (Alibert et al., 2017). Moreover, studies have shown that cell stiffness and elasticity are a direct reflection of cytoskeleton organization (Pi et al., 2013; Solon et al., 2007; Wang et al., 2016; ZHAO et al., 2015). We performed a quantitative analysis of elasticity by indenting the different

cell points with the probe, in order to extract force curves for elasticity and stiffness analyses. We found that native cells are softer compared to those treated with quercetin. This is probably due to the greater organization and exposure of the cortical actin filaments. As previously reported, the cortex actin appears to be less rigid than cytoplasmic actin filaments, which would explain the lesser rigidity of T24 cells in their native state (Laurent et al., 2003). We also observed that cells treated with quercetin lost their elastic characteristic, becoming more rigid. This result is related to the anticancer and antiproliferative effect observed by us and is in accordance with the literature, which shows that prostate cancer cells have increased stiffness after treatment with 8 different anticancer drugs. (Ren et al., 2015). It is important to note that the effects of quercetin on cell elasticity in fixed T24 cells can be transposed to living cells since the fixation processes only freeze the ongoing mechanical alterations at the moment of fixation (Targosz-Korecka et al., 2015). These findings, together with our results, corroborate that quercetin could serve as an adjuvant in bladder cancer treatment.

The study of particle size has been used to demonstrate changes in components of the plasma membrane such as biomolecules (Pi et al., 2016, 2015; Psahoulia et al., 2007). Measuring particle size provides information on ongoing physiological processes in the plasma membrane, such as ion channels opening/closing, cytoskeleton disruption and protein aggregation (Pi et al., 2016, 2015; Psahoulia et al., 2007). Ultrastructural analyses have demonstrated, for example, the reduction in cell growth receptors in MCF-7 cells after resveratrol treatment (Zhang et al., 2014). The enlarged particle size in the T24 cells induced by quercetin observed by us seems to be related to the apoptotic process since it is known that changes such as the flip-flop effect, receptor protein aggregation, and lipid rafts are involved (Demchenko, 2012). A previous study with colon cancer cells treated with quercetin showed an increase in particle size related to the apoptotic process (Psahoulia et al., 2007). The study also associates the accumulation of cell death receptors in lipid rafts with the increase in particle size, which corroborates our data (Psahoulia et al., 2007). Moreover, an increase in particle size, i.e. increased cell membrane granularity, might account for the increased stiffness observed in cells treated with quercetin (Fig. 8), which is related to cytoskeletal aggregation also common in apoptosis (Pi et al., 2016). It has been previously reported that cells treated with low quercetin concentrations accumulate F-actin, resulting in cellular shrinkage, another feature of apoptosis, found in the present study (Fig. 4) (Pi et al., 2016).

Although we did not perform cytoskeleton staining, both senescence and apoptosis are known to involve cell membrane reorganization. While cellular senescence is associated with the reorganization of the microtubule cytoskeleton (Moujaber et al., 2019), during apoptosis cells undergo characteristic morphological changes in which the cytoskeleton plays an active role (i.e. actinomyosin ring contraction) (Povea-Cabello et al., 2017). *in vitro* and *in vivo* studies reported in the literature show quercetin induces apoptosis in several types of cancer (e.g. osteosarcoma, melanoma, retinoblastoma, lung cancer, myeloma, oral cancer, among others) (Almatroodi et al., 2021; Vafadar et al., 2020). Recently, studies have reported that quercetin can induce senescence in tumor cells (Bian et al., 2020). Taken together, the evidence from the NMA and AFM analyses suggests quercetin induced the reorganization of the cytoskeleton. However, cytoskeleton staining would be necessary to prove these alterations.

5. Conclusion

Taken together, our data demonstrate quercetin has an antitumor effect in human bladder cancer cells, as observed by the reduced viability and proliferation of T24 cells. Biophysical and morphological analyses indicate this effect is a result of the apoptotic process induced by quercetin, since the treated T24 cells showed morphological alterations characteristic of apoptosis. Moreover, the absence of plasma membrane damage in quercetin-treated T24 cells suggests the cells are not dying by necrosis, but rather an ongoing death by apoptosis. Further NMA analysis found the T24 cells presented fewer normal nuclei and more nuclei with alterations commonly seen in early apoptosis, senescence, and other nuclear damaging processes, thus corroborating the apoptotic effects of quercetin. Lastly, the AFM analysis revealed a pattern of cell damage following treatment with different quercetin concentrations, gradually starting with small contour irregularities, increased number of holes and pits, cell shrinkage, and culminating in tumor cell collapse.

Finally, our study shows, for the first time, the morphological and mechanical characterization of bladder cancer T24 cells subjected to quercetin treatment and indicating an antitumor effect. We hope this study can serve as a starting point and support for other studies in the analysis of quercetin in the treatment of bladder cancer.

Funding

This work was partially funded by the Coordenação de Aperfeiçoamento de Pessoal de Nível Superior – Brasil (CAPES – Finance Code 001) and CNPq (Universal 2018- process number 409272/2018-3). The authors would like to thank CAPES and CNPq for the scholarships awarded, and PUCRS for their financial and technical support.

Declaration of Competing Interest

The authors declare that they have no known competing financial interests or personal relationships that could have appeared to influence the work reported in this paper.

Acknowledgment

We like to thank the PUCRS Central Laboratory of Microscopy and Microanalysis (LabCEMM) for the AFM analyses.

Appendix A. Supplementary data

Supplementary material related to this article can be found, in the online version, at doi:https://doi.org/10.1016/j.micron.2021.103152.

References

Alban, L., Monteiro, W.F., Diz, F.M., Miranda, G.M., Scheid, C.M., Zotti, E.R., Morrone, F. B., Ligabue, R., 2020. New quercetin-coated titanate nanotubes and their radiosensitization effect on human bladder cancer. Mater. Sci. Eng. C 110, 110662. https://doi.org/10.1016/j.msec.2020.110662.

Alibert, C., Goud, B., Manneville, J.-B., 2017. Are cancer cells really softer than normal cells? Biol. Cell 109, 167–189. https://doi.org/10.1111/boc.201600078.

Almatroodi, S.A., Alsahli, M.A., Almatroudi, A., Verma, A.K., Aloliqi, A., Allemailem, K. S., Khan, A.A., Rahmani, A.H., Bian, Y., Wei, J., Zhao, C., Li, G., Ghafouri-Fard, S., Shabestari, F.A., Vaezi, S., Abak, A., Shoorei, H., Karimi, A., Taheri, M., Basiri, A., Manuscript, A., Vafadar, A., Shabaninejad, Z., Movahedpour, A., Fallahi, F., Taghavipour, M., Ghasemi, Y., Akbari, M., Shafiee, A., Hajighadimi, S., Moradizarmehri, S., Razi, E., Savardashtaki, A., Mirzaei, H., 2021. Quercetin and cancer: new insights into its therapeutic effects on ovarian cancer cells. Cell Biosci. 26, 111548 https://doi.org/10.1186/s13578-020-00397-0.

Antoni, S., Ferlay, J., Soerjomataram, I., Znaor, A., Jemal, A., Bray, F., 2017. Bladder cancer incidence and mortality: a global overview and recent trends. Eur. Urol. https://doi.org/10.1016/j.eururo.2016.06.010.

Bambury, R.M., Rosenberg, J.E., 2013. Advanced urothelial carcinoma: overcoming treatment resistance through novel treatment approaches. Front. Pharmacol. 4, 1–7. https://doi.org/10.3389/fphar.2013.00003.

Basso, B., de, S., de Mesquita, F.C., Dias, H.B., Krause, G.C., Scherer, M., Santarém, E.R., de Oliveira, J.R., 2019. Therapeutic effect of Baccharis anomala DC. Extracts on activated hepatic stellate cells. EXCLI J. 18, 91–105. https://doi.org/10.17179/excli2018-1696.

Bastatas, L., Martinez-Marin, D., Matthews, J., Hashem, J., Lee, Y.J., Sennoune, S., Filleur, S., Martinez-Zaguilan, R., Park, S., 2012. AFM nano-mechanics and calcium dynamics of prostate cancer cells with distinct metastatic potential. Biochim. Biophys. Acta - Gen. Subj. 1820, 1111–1120. https://doi.org/10.1016/j.bbagen.2012.02.006.

Bellmunt, J., Petrylak, D.P., 2012. New therapeutic challenges in advanced bladder cancer. Semin. Oncol. 39, 598–607. https://doi.org/10.1053/j.seminoncol.2012.08.007.

Bian, Y., Wei, J., Zhao, C., Li, G., 2020. Natural polyphenols targeting senescence: a novel prevention and therapy strategy for cancer. Int. J. Mol. Sci. 21 https://doi.org/10.3390/ijms21020684.

Bortner, C.D., Cidlowski, J.A., 1998. A necessary role for cell shrinkage in apoptosis. Biochem. Pharmacol. 56, 1549–1559. https://doi.org/10.1016/S0006-2952(98)00225-1.

Buss, J.H., Begnini, K.R., Bender, C.B., Pohlmann, A.R., Guterres, S.S., Collares, T., Seixas, F.K., 2018. Nano-BCG: a promising delivery system for treatment of human bladder cancer. Front. Pharmacol. 8, 1–9. https://doi.org/10.3389/fphar.2017.00977.

Chowdhury, S.A., Kishino, K., Satoh, R., Hashimoto, K., Kikuchi, H., Nishikawa, H., Shirataki, Y., Sakagami, H., n.d. Tumor-specificity and apoptosis-inducing activity of stilbenes and flavonoids. Anticancer Res. 25, 2055–2063.

Codan, B., Del Favero, G., Martinelli, V., Long, C.S., Mestroni, L., Sbaizero, O., 2014. Exploring the elasticity and adhesion behavior of cardiac fibroblasts by atomic force microscopy indentation. Mater. Sci. Eng. C 40, 427–434. https://doi.org/10.1016/j.msec.2014.04.003.

Cross, S.E., Jin, Y.-S., Rao, J., Gimzewski, J.K., 2007. Nanomechanical analysis of cells from cancer patients. Nat. Nanotechnol. 2, 780–783. https://doi.org/10.1038/nnano.2007.388.

Demchenko, A.P., 2012. The change of cellular membranes on apoptosis: fluorescence detection. Exp. Oncol. 34, 263–268.

Dietrich, F., Figueiró, F., Filippi-Chiela, E.C., Cappellari, A.R., Rockenbach, L., Tremblay, A., de Paula, P.B., Roesler, R., Filho, A.B., Sévigny, J., Morrone, F.B., Battastini, A.M.O., 2018. Ecto-5′-nucleotidase/CD73 contributes to the radiosensitivity of T24 human bladder cancer cell line. J. Cancer Res. Clin. Oncol. 144, 469–482. https://doi.org/10.1007/s00432-017-2567-3.

Doss, B.L., Staunton, J.R., Lindsay, S.M., Ros, R., 2015. AFM indentation reveals actomyosin-based stiffening of metastatic cancer cells during invasion into collagen I matrices. Biophys. J. 108, 142a. https://doi.org/10.1016/j.bpj.2014.11.784.

Ferlay, J., Steliarova-Foucher, E., Lortet-Tieulent, J., Rosso, S., Coebergh, J.W.W., Comber, H., Forman, D., Bray, F., 2013. Cancer incidence and mortality patterns in Europe: estimates for 40 countries in 2012. Eur. J. Cancer. https://doi.org/10.1016/j.ejca.2012.12.027.

Filippi-Chiela, E.C., Oliveira, M.M., Jurkovski, B., Callegari-Jacques, S.M., Silva, V.Dda, Lenz, G., 2012. Nuclear morphometric analysis (NMA): screening of senescence, apoptosis and nuclear irregularities. PLoS One 7, e42522. https://doi.org/10.1371/journal.pone.0042522.

Hayashi, K., Iwata, M., 2015. Stiffness of cancer cells measured with an AFM indentation method. J. Mech. Behav. Biomed. Mater. 49, 105–111. https://doi.org/10.1016/j.jmbbm.2015.04.030.

Jacobs, B.L., Lee, C.T., Montie, J.E., 2010. Bladder cancer in 2010. CA Cancer J. Clin. 60, 244–272. https://doi.org/10.3322/caac.20077. Available.

Kamat, A.M., Hahn, N.M., Efstathiou, J.A., Lerner, S.P., Malmström, P.U., Choi, W., Guo, C.C., Lotan, Y., Kassouf, W., 2016. Bladder cancer. Lancet 388, 2796–2810. https://doi.org/10.1016/S0140-6736(16)30512-8.

Kim, H., Yamagishi, A., Imaizumi, M., Onomura, Y., Nagasaki, A., Miyagi, Y., Okada, T., Nakamura, C., 2017a. Quantitative measurements of intercellular adhesion between a macrophage and cancer cells using a cup-attached AFM chip. Colloids Surf. B Biointerfaces 155, 366–372. https://doi.org/10.1016/j.colsurfb.2017.04.039.

Kim, S.-O., Kim, J., Okajima, T., Cho, N.-J., 2017b. Mechanical properties of paraformaldehyde-treated individual cells investigated by atomic force microscopy and scanning ion conductance microscopy. Nano Converg. 4, 5. https://doi.org/10.1186/s40580-017-0099-9.

Lan, C.-Y., Chen, S.-Y., Kuo, C.-W., Lu, C.-C., Yen, G.-C., 2019. Quercetin facilitates cell death and chemosensitivity through RAGE/PI3K/AKT/mTOR axis in human pancreatic cancer cells. J. Food Drug Anal. 27, 887–896. https://doi.org/10.1016/j.jfda.2019.07.001.

Laurent, V.M., Fodil, R., Cañadas, P., Féréol, S., Louis, B., Planus, E., Isabey, D., 2003. Partitioning of cortical and deep cytoskeleton responses from transient magnetic bead twisting. Ann. Biomed. Eng. 31, 1263–1278. https://doi.org/10.1114/1.1616932.

Lei, C.-S., Hou, Y.-C., Pai, M.-H., Lin, M.-T., Yeh, S.-L., 2018. Effects of quercetin combined with anticancer drugs on metastasis-associated factors of gastric cancer cells: in vitro and in vivo studies. J. Nutr. Biochem. 51, 105–113. https://doi.org/10.1016/j.jnutbio.2017.09.011.

Lekka, M., Gil, D., Pogoda, K., Dulińska-Litewka, J., Jach, R., Gostek, J., Klymenko, O., Prauzner-Bechcicki, S., Stachura, Z., Wiltowska-Zuber, J., Okoń, K., Laidler, P., 2012. Cancer cell detection in tissue sections using AFM. Arch. Biochem. Biophys. 518, 151–156. https://doi.org/10.1016/j.abb.2011.12.013.

Lesjak, M., Beara, I., Simin, N., Pintać, D., Majkić, T., Bekvalac, K., Orčić, D., Mimica-Dukić, N., 2018. Antioxidant and anti-inflammatory activities of quercetin and its derivatives. J. Funct. Foods 40, 68–75. https://doi.org/10.1016/j.jff.2017.10.047.

Li, Q.S., Lee, G.Y.H., Ong, C.N., Lim, C.T., 2008. AFM indentation study of breast cancer cells. Biochem. Biophys. Res. Commun. 374, 609–613. https://doi.org/10.1016/j.bbrc.2008.07.078.

Liu, Y., Tang, Z.-G., Lin, Y., Qu, X.-G., Lv, W., Wang, G.-B., Li, C.-L., 2017. Effects of quercetin on proliferation and migration of human glioblastoma U251 cells. Biomed. Pharmacother. 92, 33–38. https://doi.org/10.1016/j.biopha.2017.05.044.

Ma, L., 2006. Growth inhibitory effects of quercetin on bladder cancer cell. Front. Biosci. 11, 2275. https://doi.org/10.2741/1970.

Ma, N., Wu, F.-G., Zhang, X., Jiang, Y.-W., Jia, H.-R., Wang, H.-Y., Li, Y.-H., Liu, P., Gu, N., Chen, Z., 2017. Shape-dependent radiosensitization effect of gold nanostructures in cancer radiotherapy: comparison of gold nanoparticles, nanospikes, and nanorods. ACS Appl. Mater. Interfaces 9, 13037–13048. https://doi.org/10.1021/acsami.7b01112.

Moch, H., Cubilla, A.L., Humphrey, P.A., Reuter, V.E., Ulbright, T.M., 2016. The 2016 WHO classification of tumours of the urinary system and male genital organs—part a: renal, penile, and testicular tumours. Eur. Urol. 70, 93–105. https://doi.org/10.1016/j.eururo.2016.02.029.

Moujaber, O., Fishbein, F., Omran, N., Liang, Y., Colmegna, I., Presley, J.F., Stochaj, U., 2019. Cellular senescence is associated with reorganization of the microtubule cytoskeleton. Cell. Mol. Life Sci. 76, 1169–1183. https://doi.org/10.1007/s00018-018-2999-1.

Pi, J., Yang, F., Jin, H., Huang, X., Liu, R., Yang, P., Cai, J., 2013. Selenium nanoparticles induced membrane bio-mechanical property changes in MCF-7 cells by disturbing membrane molecules and F-actin. Bioorganic Med. Chem. Lett. 23, 6296–6303. https://doi.org/10.1016/j.bmcl.2013.09.078.

Pi, J., Cai, H., Jin, H., Yang, F., Jiang, J., Wu, A., Zhu, H., Liu, J., Su, X., Yang, P., Cai, J., 2015. Qualitative and quantitative analysis of ROS-Mediated oridonin-induced oesophageal Cancer kyse-150 cell apoptosis by atomic force microscopy. PLoS One 10, e0140935. https://doi.org/10.1371/journal.pone.0140935.

Pi, J., Li, B., Tu, L., Zhu, H., Jin, H., Yang, F., Bai, H., Cai, H., Cai, J., 2016. Investigation of quercetin-induced HepG2 cell apoptosis-associated cellular biophysical alterations by atomic force microscopy. Scanning 38, 100–112. https://doi.org/10.1002/sca.21245.

Pietuch, A., Brückner, B.R., Janshoff, A., 2013. Membrane tension homeostasis of epithelial cells through surface area regulation in response to osmotic stress. Biochim. Biophys. Acta - Mol. Cell Res. 1833, 712–722. https://doi.org/10.1016/j.bbamcr.2012.11.006.

Povea-Cabello, S., Oropesa-Ávila, M., de la Cruz-Ojeda, P., Villanueva-Paz, M., De La Mata, M., Suárez-Rivero, J.M., Álvarez-Córdoba, M., Villalón-García, I., Cotán, D., Ybot-González, P., Sánchez-Alcázar, J.A., 2017. Dynamic reorganization of the cytoskeleton during apoptosis: the two coffins hypothesis. Int. J. Mol. Sci. 18 https://doi.org/10.3390/ijms18112393.

Psahoulia, F.H., Drosopoulos, K.G., Doubravska, L., Andera, L., Pintzas, A., 2007. Quercetin enhances TRAIL-mediated apoptosis in colon cancer cells by inducing the accumulation of death receptors in lipid rafts. Mol. Cancer Ther. 6, 2591–2599. https://doi.org/10.1158/1535-7163.MCT-07-0001.

Qu, Y., Wang, Z., Zhao, F., Liu, J., Zhang, W., Li, J., Song, Z., Xu, H., 2018. AFM-detected apoptosis of hepatocellular carcinoma cells induced by American ginseng root water extract. Micron 104, 1–7. https://doi.org/10.1016/j.micron.2017.10.003.

Raffa, D., Maggio, B., Raimondi, M.V., Plescia, F., Daidone, G., 2017. Recent discoveries of anticancer flavonoids. Eur. J. Med. Chem. 142, 213–228. https://doi.org/10.1016/j.ejmech.2017.07.034.

Ren, J., Huang, H., Liu, Y., Zheng, X., Zou, Q., 2015. An atomic force microscope study revealed two mechanisms in the effect of anticancer drugs on rate-dependent young's Modulus of human prostate cancer cells. PLoS One 10, e0126107. https://doi.org/10.1371/journal.pone.0126107.

Rockenbach, L., Bavaresco, L., Fernandes Farias, P., Cappellari, A.R., Barrios, C.H., Bueno Morrone, F., Oliveira Battastini, A.M., 2013. Alterations in the extracellular catabolism of nucleotides are involved in the antiproliferative effect of quercetin in human bladder cancer T24 cells. Urol. Oncol. Semin. Orig. Investig. 31, 1204–1211. https://doi.org/10.1016/j.urolonc.2011.10.009.

Russell, C.M., Lebastchi, A.H., Borza, T., Spratt, D.E., Morgan, T.M., 2016. The role of transurethral resection in trimodal therapy for muscle-invasive bladder cancer. Bl. Cancer 2, 381–394. https://doi.org/10.3233/BLC-160076.

Shukla, S.R., Kulkarni, K.S., 2002. Depolymerization of poly(ethylene terephthalate) waste. J. Appl. Polym. Sci. 85, 1765–1770. https://doi.org/10.1002/app.10714.

Solon, J., Levental, I., Sengupta, K., Georges, P.C., Janmey, P.A., 2007. Fibroblast adaptation and stiffness matching to Soft elastic substrates. Biophys. J. 93, 4453–4461. https://doi.org/10.1529/biophysj.106.101386.

Stevens, F.E., Beamish, H., Warrener, R., Gabrielli, B., 2008. Histone deacetylase inhibitors induce mitotic slippage. Oncogene 27, 1345–1354. https://doi.org/10.1038/sj.onc.1210779.

Sundar Rajan, V., Laurent, V.M., Verdier, C., Duperray, A., 2017. Unraveling the receptor-ligand interactions between bladder Cancer cells and the endothelium using AFM. Biophys. J. 112, 1246–1257. https://doi.org/10.1016/j.bpj.2017.01.033.

Tang, S.-M., Deng, X.-T., Zhou, J., Li, Q.-P., Ge, X.-X., Miao, L., 2020. Pharmacological basis and new insights of quercetin action in respect to its anti-cancer effects. Biomed. Pharmacother. 121, 109604 https://doi.org/10.1016/j.biopha.2019.109604.

Targosz-Korecka, M., Daniel Brzezinka, G., Danilkiewicz, J., Rajfur, Z., Szymonski, M., 2015. Glutaraldehyde fixation preserves the trend of elasticity alterations for endothelial cells exposed to TNF-α. Cytoskeleton 72, 124–130. https://doi.org/10.1002/cm.21217.

Teekaraman, D., Elayapillai, S.P., Viswanathan, M.P., Jagadeesan, A., 2019. Quercetin inhibits human metastatic ovarian cancer cell growth and modulates components of the intrinsic apoptotic pathway in PA-1 cell line. Chem. Biol. Interact. 300, 91–100. https://doi.org/10.1016/j.cbi.2019.01.008.

Trtik, P., Kaufmann, J., Volz, U., 2012. On the use of peak-force tapping atomic force microscopy for quantification of the local elastic modulus in hardened cement paste. Cem. Concr. Res. 42, 215–221. https://doi.org/10.1016/j.cemconres.2011.08.009.

Tsai, T.F., Hwang, T.I.S., Lin, J.F., Chen, H.E., Yang, S.C., Lin, Y.C., Chou, K.Y., 2019. Suppression of quercetin-induced autophagy enhances cytotoxicity through elevating apoptotic cell death in human bladder cancer cells. Urol. Sci. 30, 58–66. https://doi.org/10.4103/UROS.UROS_22_18.

Vafadar, A., Shabaninejad, Z., Movahedpour, A., Fallahi, F., Taghavipour, M., Ghasemi, Y., Akbari, M., Shafiee, A., Hajighadimi, S., Moradizarmehri, S., Razi, E., Savardashtaki, A., Mirzaei, H., 2020. Quercetin and cancer: new insights into its therapeutic effects on ovarian cancer cells. Cell Biosci. 10, 1–17. https://doi.org/10.1186/s13578-020-00397-0.

Vakifahmetoglu, H., Olsson, M., Zhivotovsky, B., 2008. Death through a tragedy: mitotic catastrophe. Cell Death Differ. 15, 1153–1162. https://doi.org/10.1038/cdd.2008.47.

van de Putte, E.E.F., Bosschieter, J., van der Kwast, T.H., Bertz, S., Denzinger, S., Manach, Q., Compérat, E.M., Boormans, J.L., Jewett, M.A.S., Stoehr, R., van Leenders, G.J.L.H., Nieuwenhuijzen, J.A., Zlotta, A.R., Hendricksen, K., Rouprêt, M., Otto, W., Burger, M., Hartmann, A., van Rhijn, B.W.G., 2018. The World Health Organization 1973 classification system for grade is an important prognosticator in T1 non-muscle-invasive bladder cancer. BJU Int. 122, 978–985. https://doi.org/10.1111/bju.14238.

van den Bosch, S., Alfred Witjes, J., 2011. Long-term cancer-specific survival in patients with high-risk, non–muscle-invasive bladder cancer and tumour progression: a systematic review. Eur. Urol. 60, 493–500. https://doi.org/10.1016/j.eururo.2011.05.045.

Vargas, J.E., Puga, R., Lenz, G., Trindade, C., Filippi-Chiela, E., 2020. Cellular mechanisms triggered by the cotreatment of resveratrol and doxorubicin in breast cancer: a translational in vitro–In silico model. Oxid. Med. Cell. Longev. 2020, 1–23. https://doi.org/10.1155/2020/5432651.

Wang, D.-C., Chen, K.-Y., Tsai, C.-H., Chen, G.-Y., Chen, C.-H., 2011. AFM membrane roughness as a probe to identify oxidative stress-induced cellular apoptosis. J. Biomech. 44, 2790–2794. https://doi.org/10.1016/j.jbiomech.2011.08.021.

Wang, Y., Xu, C., Jiang, N., Zheng, L., Zeng, J., Qiu, C., Yang, H., Xie, S., 2016. Quantitative analysis of the cell-surface roughness and viscoelasticity for breast cancer cells discrimination using atomic force microscopy. Scanning 38, 558–563. https://doi.org/10.1002/sca.21300.

Zhang, L., Yang, F., Cai, J.-Y., Yang, P.-H., Liang, Z.-H., 2014. In-situ detection of resveratrol inhibition effect on epidermal growth factor receptor of living MCF-7 cells by Atomic Force Microscopy. Biosens. Bioelectron. 56, 271–277. https://doi.org/10.1016/j.bios.2014.01.024.

Zhao, S., Stamm, A., Lee, J.S., Gruverman, A., Lim, J.Y., Gu, L., 2015. Elasticity of differentiated and undifferentiated human neuroblastoma cells characterized by atomic force microscopy. J. Mech. Med. Biol. 15, 1550069 https://doi.org/10.1142/S0219519415500694.

Zhao, J., Fang, Z., Zha, Z., Sun, Q., Wang, H., Sun, M., Qiao, B., 2019. Quercetin inhibits cell viability, migration and invasion by regulating miR-16/HOXA10 axis in oral cancer. Eur. J. Pharmacol. 847, 11–18. https://doi.org/10.1016/j.ejphar.2019.01.006.

Ziegler, U., Groscurth, P., 2004. Morphological features of cell death. Physiology 19, 124–128. https://doi.org/10.1152/nips.01519.2004.